

# Cresting the wave: proper motions of the Eastern Banded Structure

Alis J. Deason,<sup>1</sup>★ Vasily Belokurov<sup>2</sup> and Sergey E. Koposov<sup>2,3</sup>

<sup>1</sup>*Institute for Computational Cosmology, Department of Physics, University of Durham, South Road, Durham DH1 3LE, UK*

<sup>2</sup>*Institute of Astronomy, University of Cambridge, Madingley Road, Cambridge CB3 0HA, UK*

<sup>3</sup>*McWilliams Center for Cosmology, Department of Physics, Carnegie Mellon University, 5000 Forbes Avenue, Pittsburgh, PA 15213, USA*

Accepted 2017 September 26. Received 2017 September 22; in original form 2017 July 29

## ABSTRACT

We study the kinematic properties of the Eastern Banded Structure (EBS) and Hydra I overdensity using exquisite proper motions derived from the Sloan Digital Sky Survey (SDSS) and *Gaia* source catalogue. Main sequence turn-off stars in the vicinity of the EBS are identified from SDSS photometry; we use the proper motions and, where applicable, spectroscopic measurements of these stars to probe the kinematics of this apparent stream. We find that the EBS and Hydra I share common kinematic and chemical properties with the nearby Monoceros Ring. In particular, the proper motions of the EBS, like Monoceros, are indicative of prograde rotation ( $V_\phi \sim 180\text{--}220 \text{ km s}^{-1}$ ), which is similar to the Galactic thick disc. The kinematic structure of stars in the vicinity of the EBS suggests that it is not a distinct stellar stream, but rather marks the ‘edge’ of the Monoceros Ring. The EBS and Hydra I are the latest substructures to be linked with Monoceros, leaving the Galactic anti-centre a mess of interlinked overdensities which likely share a unified, Galactic disc origin.

**Key words:** Galaxy: halo – Galaxy: kinematics and dynamics – Galaxy: structure.

## 1 INTRODUCTION

Galaxies like the Milky Way consume and destroy several lower mass dwarf galaxies over their lifetime. Evidence of these fatal accretion events can be seen in the form of streams, clouds, shells and incoherent blobs that litter the stellar halo (e.g. Belokurov et al. 2006). The interaction between accreted dwarf galaxies and the Galactic disc cannot only rip apart the dwarf, but can perturb, warp and even ‘kick out’ stars from the stellar disc (e.g. Velazquez & White 1999; Benson et al. 2004; Purcell, Bullock & Kazantzidis 2010).

A stunning example of a substructure at the disc–halo interface, is the so-called Monoceros Ring. This local ( $D \sim 10 \text{ kpc}$ ) overdensity located close to the Galactic anti-centre was first uncovered by Newberg et al. (2002) using imaging data from the Sloan Digital Sky Survey (SDSS; York et al. 2000), and the ring-like structure was later confirmed by Ibata et al. (2003). There are two main formation scenarios that have been put forward to explain this vast anti-centre structure: (1) tidal debris from a disrupted dwarf galaxy and (2) a perturbation of the Galactic disc. Subsequent scrutiny of the anti-centre region has uncovered yet more substructure that could be related to Monoceros: the Canis Major overdensity, which has been touted as a potential progenitor of Monoceros (Martin et al. 2004), the Eastern Banded Structure (EBS), the anti-centre stream (ACS) (Grillmair 2006) and a Southern counterpart to

Monoceros at larger distances ( $D > 15 \text{ kpc}$ ) called TriAnd (Majewski et al. 2004; Rocha-Pinto et al. 2004). More recently it has been suggested that the disc in this region has complex substructure, which is caused by an accreted dwarf galaxy. Thus, these apparently spatially separated substructures could have a unified origin (see e.g. Slater et al. 2014; Xu et al. 2015). In this paper, we focus on the EBS, a faint, short structure first discovered by Grillmair (2006). Despite its proximity to Monoceros, a re-analysis by Grillmair (2011) found that the EBS was unlikely related to the Ring, and is instead a distinct stellar stream. Indeed, Grillmair (2011) suggested that a relatively high surface density, double-lobed feature found along the stream—called Hydra I—could be the dwarf galaxy or globular cluster progenitor of the stream. However, while the shallow SDSS imaging assumed an old, metal-poor stellar population, deeper imaging and spectroscopy of Hydra I by Hargis et al. (2016) revealed that this overdensity is of intermediate age (5–6 Gyr) and metallicity ( $[\text{Fe}/\text{H}] = -0.9$ ). This relatively high metallicity is reminiscent of the Monoceros Ring ( $[\text{Fe}/\text{H}] \sim -1.0$ , e.g. Ivezić et al. 2008; Meisner et al. 2012), which is only slightly more metal-poor than the thick disc ( $[\text{Fe}/\text{H}] \sim -0.7$ , e.g. Gilmore & Wyse 1985).

It is clear that a kinematic exploration of the anti-centre region is desperately needed to dissect these complex structures. To this end, de Boer, Belokurov & Koposov (2017) recently exploited a proper motion catalogue constructed from the SDSS and first data release of *Gaia* to infer the tangential motions of the Monoceros Ring. In this paper, we use the same SDSS–*Gaia* catalogue to examine the kinematics of the EBS and Hydra I, and relate them to the Ring.

\* E-mail: [alis.j.deason@durham.ac.uk](mailto:alis.j.deason@durham.ac.uk)

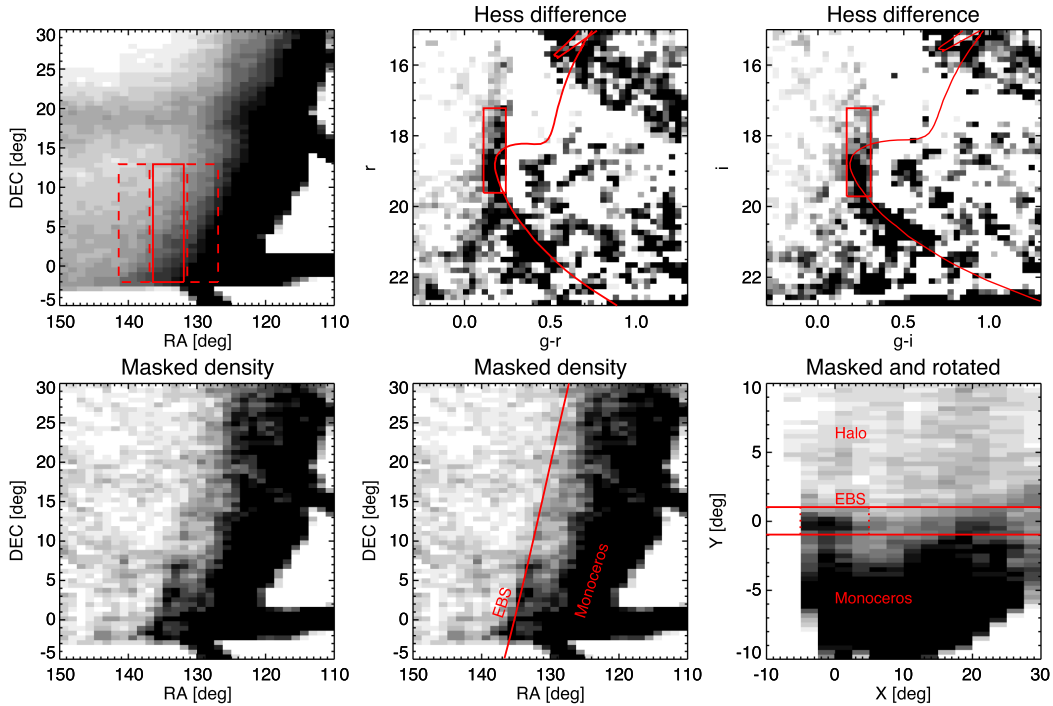


**Figure 1.** Top left panels: density map of SDSS stars in equatorial coordinates. Only stars with main sequence colours ( $0.2 < g - r < 0.6$ ) in the magnitude range  $17 < r < 22$  are shown. The red box indicates the EBS and the dashed boxes show the regions used to calculate the background. Top middle and right panels: Hess diagrams in  $g - r, r$  (middle) and  $g - i, i$  (right) colour–magnitude space. Here, we show the difference between stars in the EBS region and the background. The red box indicates the turn-off feature associated with the EBS, and the red line shows a 5.6 Gyr,  $[\text{Fe}/\text{H}] = -0.9$  isochrone at  $D = 12.7$  kpc. Bottom left and middle panels: the density of turn-off stars selected in the colour and magnitude ranges:  $0.11 < g - r < 0.24$ ,  $17.2 < r < 19.6$ ,  $0.17 < g - i < 0.31$ ,  $17.2 < i < 19.7$ . The red line in the bottom middle panel shows a great circle through the EBS. Bottom right panel: density of turn-off stars in a coordinate system with equator aligned with the EBS stream. Hydra I lies at  $X, Y = [0, 0]$  deg. The solid red line indicates the approximate boundary of the EBS stream,  $|Y| < 1.0$  deg, and the dotted line shows the range along the stream where there is obvious EBS signal ( $|X| < 5$  deg).

## 2 SDSS-GAIA PROPER MOTIONS

In order to examine the proper motions of the EBS, we use a newly calibrated SDSS–*Gaia* catalogue (Koposov et al., in preparation). The details of the creation of the recalibrated SDSS astrometric catalogue, the measurement of SDSS–*Gaia* proper motions and the statistical and systematic uncertainties of the derived proper motions, are described in more detail in Koposov et al. (in preparation), Deason et al. (2017) and de Boer et al. (2017). Here, we give a very brief description.

A comparison between the positions of stars in the SDSS Data Release 10 (Ahn et al. 2014) and the *Gaia* source catalogue (Gaia Collaboration et al. 2016) with a baseline of  $\sim 5$ – $10$  yr can potentially yield proper motions across a large area of sky. However, there are several systematics present in this naive cross-match, particularly due to the astrometric solution of the SDSS survey. To this end, Koposov et al. (in preparation) recalibrate the SDSS astrometry based on the excellent astrometry of the *Gaia* source catalogue. These recalibrated positions are then cross-matched with the *Gaia* catalogue resulting in proper motion measurements for the majority of sources down to  $r \sim 20$  mag. The precision of the new SDSS–*Gaia* proper motions are examined in Deason et al. (2017) and de Boer et al. (2017) using spectroscopically confirmed QSOs. The systematics of the catalogue are very low ( $\sim 0.1$  mas yr $^{-1}$ ) and the statistical uncertainties are typically  $1.5$  mas yr $^{-1}$ . In this work, we adopt the proper motion uncertainties as a function of magnitude derived by de Boer et al.

(2017) for the anti-centre region:  $\sigma_{\mu_l} = 36.04 - 3.867g + 0.107g^2$ ,  $\sigma_{\mu_b} = 26.50 - 2.894g + 0.082g^2$ .

## 3 SAMPLE SELECTION

In this Section, we outline our selection of stars associated with the EBS. In Fig. 1, we show how EBS stars are identified according to their position on the sky, colour and magnitude. The top left panel shows a density map of SDSS stars in the vicinity of the EBS. Here, only stars with main sequence colours ( $0.2 < g - r < 0.6$ ) in the magnitude range  $17 < r < 22$  are shown. The high density of stars at  $\text{RA} \sim 110$ – $130$  deg is due to the Monoceros overdensity. The solid red box indicates the region of the EBS, and the dashed red boxes show the background regions we use to make differential Hess diagrams. The Hess difference between the EBS and the background is shown in the middle and right panels. We indicate our selection of main sequence turn-off stars with the red box. There is an obvious signal of turn-off stars in the EBS relative to the background. Hargis et al. (2016) (H16 hereafter) use deeper imaging with DECam to show that Hydra I has a well-defined main sequence turn-off of intermediate age ( $\sim 5$ – $6$  Gyr) and metallicity ( $[\text{Fe}/\text{H}] = -0.9$ ). Indeed, the red line shows that a 5.6 Gyr,  $[\text{Fe}/\text{H}] = -0.9$  isochrone at the distance of Hydra I ( $D = 12.7$  kpc) agrees well with the turn-off signal in the EBS. In the bottom left and middle panels, we show the density of stars on the sky, which are selected to have the same colour and magnitude as the EBS turn-off. These colour and

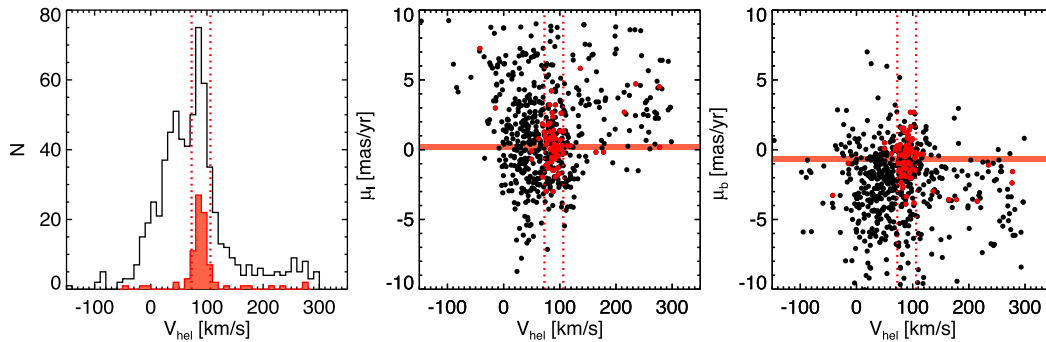


**Figure 2.** Sample of  $N = 675$  candidate Hydra I stars in the SDSS–*Gaia* catalogue with spectroscopic measurements from (Hargis et al. 2016) (H16). Left-hand panel: distribution of heliocentric velocities of the H16 sample (black histogram). The shaded red histogram shows the  $N = 84$  stars that lie within our colour and magnitude selection boundaries. These stars have a narrowly peaked velocity distribution with median  $V_{\text{hel}} = 89 \text{ km s}^{-1}$ , in excellent agreement with H16. For our proper motion measurements we use the  $N = 65$  stars that have heliocentric velocities within  $2\sigma_v = 2 \times 8.4 \text{ km s}^{-1}$  of the average Hydra I velocity. Middle and right-hand panels: the Galactic proper motions of the H16 sample as a function of heliocentric velocity. The stars that pass our turn-off selection cut are shown in red. The median proper motions for the turn-off stars with  $V_{\text{hel}}$  within  $2\sigma_v$  of the net Hydra I velocity are shown with the red shaded regions. Here, the width of the lines indicate the  $1\sigma$  errors of the medians.

magnitude constraints are given by:

$$\begin{aligned} 0.11 < g - r < 0.24 \\ 17.2 < r < 19.6 \\ 0.17 < g - i < 0.31 \\ 17.2 < i < 19.7 \end{aligned} \quad (1)$$

The EBS now becomes clear in these panels, and the red line in the bottom middle panel shows an approximate great circle through the EBS (with pole at RA, Dec =  $[-134.5, 14.8]$  deg). In the bottom right panel, we transform to a coordinate system aligned with this great circle, with Hydra I at the origin ( $X, Y = [0, 0]$  deg). Here, the EBS signal is apparent at  $|X| < 5$  deg along the stream and is approximately confined to  $|Y| < 1.0$  deg.

In the following sections, we use turn-off stars selected according to equation (1) to identify EBS stars and use the rotated ( $X, Y$ ) coordinate system to dissect this structure in proper motion space.

#### 4 PROPER MOTION OF HYDRA I

Before we turn our attention to the full extent of the EBS, we focus on the potential progenitor of this stream, Hydra I. Here, we use the spectroscopic sample of stars associated with Hydra I compiled by H16, and cross-match these stars with our SDSS–*Gaia* proper motion catalogue. The top left panel of Fig. 2 shows the distribution of heliocentric velocities of the  $N = 675$  candidate Hydra I stars. The filled red histogram shows the  $N = 84$  turn-off stars that lie within the colour and magnitude selection boundaries given in equation (1).

H16 find a (probability weighted) systemic velocity of  $V_{\text{hel}} = 89.4 \text{ km s}^{-1}$  for Hydra I, with dispersion  $\sigma_v = 8.4 \text{ km s}^{-1}$ . Our turn-off star criteria produces a well-defined peak centred on this systemic velocity, and thus is clearly effective at isolating stars associated with Hydra I. The dotted lines in this panel indicate the  $2\sigma$  boundaries of the Hydra I heliocentric velocity distribution.

The middle and right-hand panels of Fig. 2 show the Galactic proper motion components of the candidate Hydra I stars. Stars that fall into our turn-off selection are highlighted in red, and the dotted red lines indicate the  $2\sigma_v$  boundary of the systemic velocity of Hydra I. Using the  $N = 65$  turn-off selected stars that have heliocentric velocities within  $2\sigma_v$  of Hydra I, we find median proper motions of:  $\mu_l = 0.18 \pm 0.21 \text{ mas yr}^{-1}$  and  $\mu_b = -0.67 \pm 0.21 \text{ mas yr}^{-1}$ .

The median values, and uncertainties in the medians, are calculated using a bootstrap method that takes into account the proper motion uncertainties of the SDSS–*Gaia* sample.

We can convert our derived proper motions and the line-of-sight velocity of Hydra I into a 3D velocity. Heliocentric quantities are converted to Galactocentric ones using a solar motion of  $v_{\phi, \odot} = 238 \text{ km s}^{-1}$  and  $(U, V, W) = (11.1, 12.24, 7.25) \text{ km s}^{-1}$  from Reid & Brunthaler (2004) and Schönrich, Binney & Dehnen (2010). Adopting a distance to Hydra I of 12.7 kpc, we find:  $(v_r, v_{\theta}, v_{\phi}) = (-22 \pm 5, -24 \pm 12, 179 \pm 12) \text{ km s}^{-1}$ . Thus, the kinematics of Hydra I indicate a prograde orbit, with similar amplitude to the Galactic thick disc.

## 5 KINEMATICS OF THE EASTERN BANDED STRUCTURE

### 5.1 Proper motion properties

We now examine the proper motions of stars in the vicinity of the EBS. Here, we only use turn-off stars (see Fig. 1 and equation 1) and use a rotated coordinate system aligned with a great circle through the EBS. In the top panels of Fig. 3, we show the median Galactic longitude (left-hand panels) and latitude (right-hand panels) proper motions of stars close to the EBS in bins of  $X$  and  $Y$ . Here, Hydra I is located at the origin ( $|X| < 1$  deg,  $|Y| < 1$  deg), and the star symbol indicates its estimated proper motion found in the previous section. For comparison, we show the proper motions of stars in the Galaxia model (Sharma et al. 2011) in the bottom panels. These stars are selected according to the same criteria as the EBS stars, and the model is dominated by halo stars in this region of the sky.

The proper motion structure in the vicinity of the EBS shows a sharp transition at  $Y \sim 0$  deg that is not apparent in the Galaxia model. The  $Y$  coordinate runs perpendicular to the stream, and the Monoceros Ring dominates at  $Y < 0$  deg. Thus, the EBS seems to mark the ‘edge’ of the Monoceros feature, and indeed the EBS proper motions (at  $|Y| < 1.0$  deg and  $1 < |X|/\text{deg} < 5$ ) are very similar to Monoceros. In Fig. 1, the density of the anti-centre features vary considerably with Galactic latitude (i.e. the EBS stands out as an obvious overdensity). Thus, if the EBS was a distinct structure, we would also expect to see a variation, or discontinuity, in the proper motions. Instead, we find that the proper motions in the vicinity of the EBS follow on continuously from the Monoceros

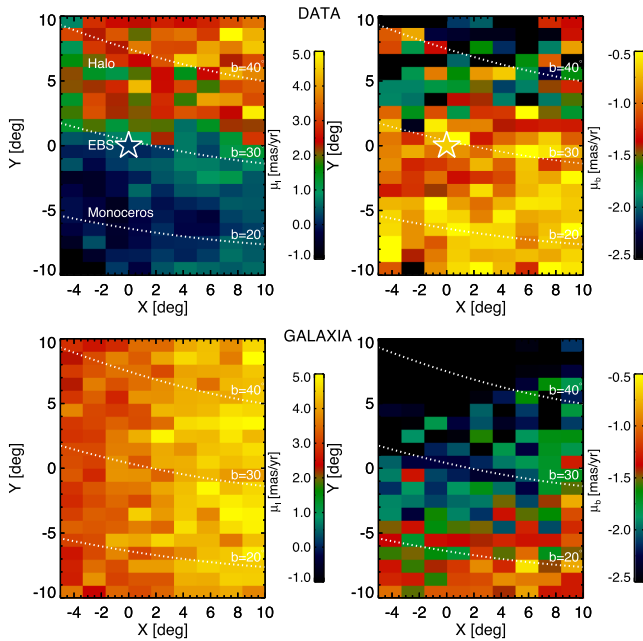


**Figure 3.** Top panels: the median proper motions of turn-off stars in the vicinity of the EBS. The coordinate system has equator aligned with the EBS, and we show lines of constant Galactic latitude. The density of EBS stars is strongest in the region  $|Y| < 1.0$  deg and  $|X| < 5$  deg. The left-hand and right-hand panels show the Galactic longitude and latitude proper motion components, respectively. At negative  $Y$  the Monoceros Ring dominates, and at positive  $Y$  the halo population becomes more apparent. The EBS is at the ‘edge’ of Monoceros and its proper motions indicate a very similar kinematic signature to the Monoceros Ring. The colour of the star symbols indicate the proper motion of Hydra I calculated in Section 4. The bottom panels show the proper motion distributions for the Galaxia model, where stars have been selected using the same colour and magnitude cuts. Note that the gradient in  $\mu_b$  along  $Y$  in Galaxia is largely due to solar reflex motion. The rotation component is mainly in the  $\mu_l$  direction hence this coordinate is more discriminating between rotation and non-rotation than  $\mu_b$  or  $V_{\text{hel}}$ .

Ring, as would be expected if the Monoceros star counts continue to dominate out to the EBS.

The transition between Monoceros and the halo can be seen more clearly in Fig. 4, where we collapse the  $X$  dimension (along the stream) and only use stars with  $1 < |X| < 5$  deg. Note that we restrict to  $|X| > 1$  deg to exclude Hydra I stars. Here, we show how the Galactic proper motion components vary perpendicular to the stream. The filled points show the median values (with associated errors) and the solid lines indicate the  $1\sigma$  dispersion. The orange star symbol indicates Hydra I, and the dot–dashed blue line shows the prediction from the Galaxia model. The solid red region shows a simple disc model with rotation  $V_\phi = 220 \text{ km s}^{-1}$  at  $D = 12.7$  kpc, where we assume the distance to EBS is the same as Hydra I. We have also included a non-rotating component, which contributes between 0–40 per cent to the model. Here, we assume a range of distances between 5 and 100 kpc that follow a power-law density distribution with slope  $-3.5$ . Note that de Boer et al. (2017) found that contamination from the Milky Way varies between 20–40 per cent in the region of the sky that is dominated by Monoceros.

The model with prograde rotation  $V_\phi = 220 \text{ km s}^{-1}$  at  $D = 12.7$  kpc follows the Monoceros stars, in good agreement with the prograde models derived by de Boer et al. (2017) for the Ring in this region of the sky (see figs 10 and 11 in de Boer et al. 2017).

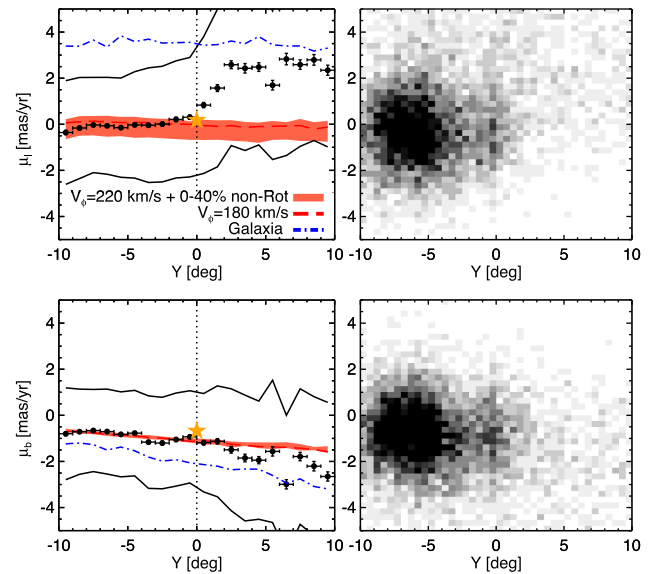


**Figure 4.** Left-hand panels: Galactic proper motions along the  $Y$  coordinate perpendicular to the EBS stream direction. We only use stars with  $1 < |X|/\text{deg} < 5$ . The black points show the median values and the solid lines indicate the  $1\sigma$  dispersion. The horizontal and vertical error bars on the black points indicate the bin size and error in the median, respectively. The yellow star indicates the values for Hydra I. The proper motions of stars in the EBS (at  $Y \sim 0$  deg) closely follow the kinematic signature of the Monoceros Ring, which dominates at  $Y < 0$  deg. The vertical dotted black line indicates the Monoceros/EBS to halo transition, and the dot–dashed blue line shows the predictions of the Galaxia model. The dashed red line indicates a simple disc model with  $V_\phi = 180 \text{ km s}^{-1}$  at  $D = 12.7$  kpc. The solid red region indicates a disc model with  $V_\phi = 220 \text{ km s}^{-1}$ , which includes a fraction of non-rotating (i.e. halo) stars that varies from 0–40 per cent. Right-hand panels: density map of proper motions as a function of  $Y$ .

However, the stars nearby to the EBS also lie close to this prograde model. Indeed, it is only at  $Y \gtrsim 2$ , beyond the EBS, that the proper motions transition to a more halo-like population.

## 5.2 Metallicity and line-of-sight velocity

For our final kinematic examination of the EBS, we isolate turn-off stars in the vicinity of the EBS with spectroscopic measurements from SDSS. Here, we adopt the spectroscopic parameters derived from the Sloan Extension for Galactic Exploration and Understanding (SEGUE, Yanny et al. 2009) Stellar Parameter Pipeline (SSPP, Lee et al. 2008). In the region  $|X| < 10$ ,  $|Y| < 10$ , there are  $N = 817$  stars with line-of-sight velocity and metallicity measurements. In Fig. 5, we show the median heliocentric velocity (top panel) and metallicity (bottom panel) in bins perpendicular to the stream (note only stars with  $|X| < 5$  deg are used). Similarly to Fig. 4, the spectroscopic properties of the EBS are similar to the Monoceros Ring, which dominates the  $Y < 0$  deg star counts. The heliocentric velocity of the EBS is indicative of a prograde rotating model with  $V_\phi \sim 180\text{--}220 \text{ km s}^{-1}$ . In addition, the EBS stars are relatively metal-rich ( $[\text{Fe}/\text{H}] \sim -0.9$ ) in good agreement with what H16 found for Hydra I. It is only beyond the EBS ( $Y \gtrsim 2$  deg) that the metallicity more closely resembles a metal-poor halo population.

## 6 SUMMARY AND DISCUSSION

In this paper, we have examined the kinematic properties of the EBS and Hydra I using exquisite proper motions derived from the

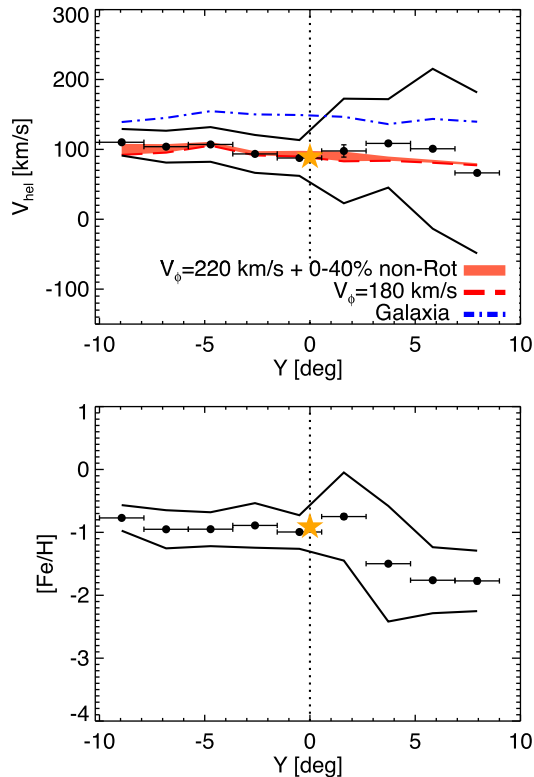


**Figure 5.** The heliocentric velocity (top panel) and metallicity (bottom panel) of stars in the vicinity of the EBS. Here, stars in SDSS with spectroscopy have been selected according to the colour and magnitude boundaries described in Fig. 1. The yellow stars indicate the values for Hydra I derived by (Hargis et al. 2016). The EBS at  $Y \sim 0$  deg has similar heliocentric velocity and metallicity as the Monoceros Ring. When  $Y > 0$  deg, the distribution transitions to the metal-poor halo. The dotted black line indicates the Monoceros/EBS to halo transition.

SDSS and *Gaia* source catalogue. We find that the EBS and Hydra I share common kinematic and chemical properties with the Monoceros Ring; the proper motions, line-of-sight velocity, distance and metallicity of the EBS *all* closely resemble Monoceros and do not appear like a halo population. In particular, the proper motions of the EBS, like Monoceros, are indicative of prograde rotation, which only slightly lags behind the Galactic thin disc. At higher Galactic latitudes than the EBS, the stellar field transitions to a halo dominated population. Thus, we conclude that the EBS is not a distinct stellar stream, but rather marks the ‘edge’ of the Monoceros Ring.

A detailed kinematic analysis of the Galactic anti-centre was recently performed by de Boer et al. (2017). These authors used the same SDSS–*Gaia* proper motion catalogue described in this work, and find that the Monoceros Ring has a prograde rotation signal with  $V_{\phi} \sim 220\text{--}240 \text{ km s}^{-1}$ . de Boer et al. (2017) also map the proper motion structure of the ACS, and although they find that it is distinct from Monoceros, the ACS has similar kinematic properties and likely shares a common origin with the Ring. There are two leading formation mechanisms for the Monoceros structure: (1) a disrupted dwarf galaxy and (2) a perturbation of the Galactic disc. de Boer et al. (2017) suggest that their results indicate a mix of these two scenarios, where both are likely needed to explain the complex structures in the anti-centre.

Our results point to yet another Galactic sub-structure associated with the Monoceros Ring. Indeed, the kinematic structure of the EBS could be likened to the ‘crest’ of the Monoceros wave. We

also find that Hydra I, the presumed progenitor of the EBS, is both kinematically and chemically related to both the EBS and Monoceros. The fact that these substructures, in addition to the ACS, are not substantially different from Monoceros puts the disrupted dwarf scenario into serious doubt. Indeed, the main remaining evidence for the debris of an accreted satellite are the reported detections of thin substructures in the anti-centre region (like EBS). Thus, our finding that the EBS is in fact not a distinct stream, and is instead an overdensity related to Monoceros, indicates that the similarity of the various stellar components in the anti-centre favors a unified, disc origin.

The Galactic anti-centre is proving to be a region of the Galaxy littered with multiple, interlinked sub-structures. This unique probe of the disc/halo interface not only allows us to study the disruption of dwarf galaxies, but also the synergy between accretion events and the response of the Galactic disc. With the advent of more detailed kinematics from *Gaia* and upcoming spectroscopic surveys (such as DESI and WEAVE; Dalton et al. 2012; DESI Collaboration et al. 2016), we can hope to piece together the complex formation scenario of Monoceros and its denizens.

## ACKNOWLEDGEMENTS

We thank an anonymous referee for a thorough report, which improved the clarity of this manuscript. AD is supported by a Royal Society University Research Fellowship. The research leading to these results has received funding from the European Research Council under the European Union’s Seventh Framework Programme (FP/2007-2013) / ERC grant agreement no. 308024. VB and SK acknowledge financial support from the ERC. AD and SK also acknowledge the support from the STFC (grants ST/P000541/1 and ST/N004493/1).

## REFERENCES

- Ahn C. P. et al., 2014, *ApJS*, 211, 17  
 Belokurov V. et al., 2006, *ApJ*, 642, L137  
 Benson A. J., Lacey C. G., Frenk C. S., Baugh C. M., Cole S., 2004, *MNRAS*, 351, 1215  
 Dalton G. et al., 2012, in McLean I. S., Ramsay S. K., Takami H., eds, *Proc. SPIE Conf. Ser. Vol. 8446, Ground-based and Airborne Instrumentation for Astronomy IV*. SPIE, Bellingham, p. 84460P  
 de Boer T. J. L., Belokurov V., Koposov S. E., 2017, *MNRAS*, preprint (arXiv:1706.09468)  
 Deason A. J., Belokurov V., Koposov S. E., Gómez F. A., Grand R. J., Marinacci F., Pakmor R., 2017, *MNRAS*, 470, 1259  
 DESI Collaboration et al., 2016, preprint (arXiv:1611.00036)  
 Gaia Collaboration et al., 2016, *A&A*, 595, A2  
 Gilmore G., Wyse R. F. G., 1985, *AJ*, 90, 2015  
 Grillmair C. J., 2006, *ApJ*, 651, L29  
 Grillmair C. J., 2011, *ApJ*, 738, 98  
 Hargis J. R. et al., 2016, *ApJ*, 818, 39 (H16)  
 Ibata R. A., Irwin M. J., Lewis G. F., Ferguson A. M. N., Tanvir N., 2003, *MNRAS*, 340, L21  
 Ivezić Ž. et al., 2008, *ApJ*, 684, 287  
 Lee Y. S. et al., 2008, *AJ*, 136, 2022  
 Majewski S. R., Ostheimer J. C., Rocha-Pinto H. J., Patterson R. J., Guhathakurta P., Reitzel D., 2004, *ApJ*, 615, 738  
 Martin N. F., Ibata R. A., Bellazzini M., Irwin M. J., Lewis G. F., Dehnen W., 2004, *MNRAS*, 348, 12  
 Meisner A. M., Frebel A., Jurić M., Finkbeiner D. P., 2012, *ApJ*, 753, 116  
 Newberg H. J. et al., 2002, *ApJ*, 569, 245  
 Purcell C. W., Bullock J. S., Kazantzidis S., 2010, *MNRAS*, 404, 1711  
 Reid M. J., Brunthaler A., 2004, *ApJ*, 616, 872

Rocha-Pinto H. J., Majewski S. R., Skrutskie M. F., Crane J. D., Patterson R. J., 2004, *ApJ*, 615, 732  
Schönrich R., Binney J., Dehnen W., 2010, *MNRAS*, 403, 1829  
Sharma S., Bland-Hawthorn J., Johnston K. V., Binney J., 2011, *ApJ*, 730, 3  
Slater C. T. et al., 2014, *ApJ*, 791, 9  
Velazquez H., White S. D. M., 1999, *MNRAS*, 304, 254

Xu Y., Newberg H. J., Carlin J. L., Liu C., Deng L., Li J., Schönrich R., Yanny B., 2015, *ApJ*, 801, 105  
Yanny B. et al., 2009, *AJ*, 137, 4377  
York D. G. et al., 2000, *AJ*, 120, 1579

This paper has been typeset from a  $\text{\TeX/L\AA\TeX}$  file prepared by the author.